Critical fluid injection volumes for uncontrolled fracture ascent.

Timothy Davis[1], **Eleonora Rivalta**[1], **Torsten Dahm**[1]

[1]GFZ (GeoForschungsZentrum), Physics of Earthquakes and Volcanoes, Helmholtzstraße 6/7, Building H 7, 14467 Potsdam. {davis,rivalta,dahm}@gfz-potsdam.de

Key Points:

- Three-dimensional threshold volumes for self-sustained fluid-filled fracture ascent
- We derive analytical equation and validate it through numerical boundary-element simulations
- Assessing safe hydro-fracture operation volumes requires quantitative modeling of in-situ complexities

Corresponding author: Timothy Davis, `davis@gfz-potsdam.de`

Abstract

Hydro-fracturing is a routine industrial technique whose safety depends on fractures remaining confined within the target rock volume. Both observations and theoretical models show that, if the fluid volume is larger than a critical value, pockets of fluid can propagate large distances in the Earth's crust in a self-sustained, uncontrolled manner. Existing models for such critical volumes are unsatisfactory, most are two-dimensional and depend on poorly constrained parameters (typically the fracture length). Here we derive both analytically and numerically in three dimensions scale-independent critical volumes as a function of only rock and fluid properties. We apply our model to gas, water and magma injections in laboratory, industrial and natural settings, showing that our critical volumes are consistent with observations and can be used as conservative estimates. We discuss competing mechanisms promoting fracture arrest, whose quantitative study could help to assess more comprehensively the safety of hydro-fracturing operations.

Plain Language Summary

Fractures in rocks can act as channels for fluids. Fracking, or hydro-fracturing, involves injection of fluids at high pressure in order to grow fractures within the rock and increase its permeability. Fluid volumes need to be kept below a threshold value: if the fluid volume is larger, then the stresses at the tips of the fluid pocket will be large enough for the fluids force their way around by fracturing the rock ahead of them. Previous theoretical models for the critical volumes are unsatisfactory as they are two-dimensional and based on poorly constrained parameters. We derive and test a new three-dimensional equation that uses only rock and fluid parameters. We find that typical volumes injected in hydro-fracturing operations are over the limit we define. We argue they are still mostly safe as additional processes often hinder fracture growth. Further work is needed to comprehensively quantify mechanisms that hinder hydro-fracture arrest.

1 Introduction

Official guidelines for hydraulic fracturing (e.g., Mair et al., 2012; EPA, 2016), outline safe operational practices for regulators. Such reports often state that during routine operations fractures are unlikely to grow out of the target rock formation, as typical injection pressures are too low for this to occur. These claims are substantiated with empirical observations from closed access microseismic data of scarce vertical fracture growth following injection (Fisher & Warpinski, 2012). Evidence for unsafe vertical migration of such fluids remains ambiguous (Vidic et al., 2013).

Natural analogues of fluid migration by hydro-fracturing include drainage crevasses in melting glaciers and magma transport by dyking. Field and experimental observations provide some indication of typical rates of fracture ascent, in the order of mm/s to around half a m/s (Das et al., 2008; Tolstoy et al., 2006). For water-filled fractures in rock this has not been observed; estimates from geochemical analysis supply similar rates of $\sim$0.01-0.1 m/s, (1 km/day) (Okamoto & Tsuchiya, 2009). Theoretical arguments suggest that the migration velocity should have a dependency on volume (Heimpel & Olson, 1994; Dahm, 2000).

According to theory, tip-propagation occurs when a critical amount of fluid has accumulated inducing enough stress to overcome the medium's fracture toughness, K_c (Secor & Pollard, 1975). So far, critical 'volumes' are given in terms of the fracture length, which is not directly observable and difficult to estimate from observations (Secor & Pollard, 1975; Dahm, 2000; Taisne et al., 2011); moreover, such analyses have been carried out in 2D only, not capturing the fracture's 3D shape and scaling of volume vs length.

Figure 1. A) Stress vs depth in the crust, data from Bell et al. (1990), crack shown in red with length $2c$. B) Stress boundary conditions and 3D crack wall displacement. C) Cross sections of crack wall displacement, itp=interpenetration. D) Shape of an ascending air filled crack in gelatine from (Rivalta & Dahm, 2006). E) Air filled cracks tip-line vs a penny-shaped tip-line.

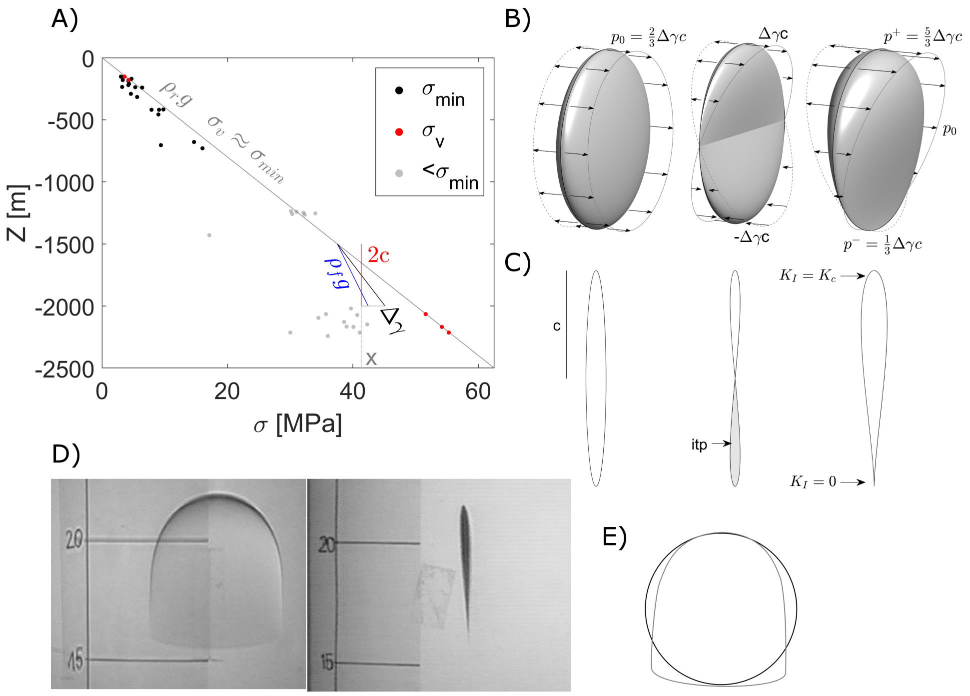

Here, after deriving a theoretical model and validating it with numerical simulations, we apply this to cracks filled with air, water, oil and magma in solids of varying stiffness and toughness, across a wide range of length scales.

Methods

1.1 Hydrofracturing and stress gradients

We consider a pressurised penny-shaped crack of radius c and volume V in an elastic medium. The crack can only grow when the stress intensity K_I at its tip-line exceeds K_c. The elastic parameters of the medium (shear modulus, μ, and Poisson's ratio, ν) control the fracture's aperture. The internal pressure p_0 must overcome the stress normal to the crack walls (generally the minimum compressive stress, σ_{min}) by an amount accommodating the volume V against the elastic forces, Fig. 1A/B.

When the crack is vertical, the gradient in the normal stress acting to close the crack and the gradient in the load due to the overlying fluid acting to open the crack, i.e. $\rho_r g$ and $\rho_f g$ in Fig. 1A, where ρ_r and ρ_f are the densities of the host rock and fluid, respectively, result in a net stress gradient $\Delta\gamma$ acting to push open the crack walls in an inverse 'teardrop' shape, Fig. 1B/C. When the crack is inclined $\Delta\gamma$ needs to be adjusted by $cos(\theta)$, where θ is the cracks' angle away from vertical. Quantitative formulations used to assess industrial fracture heights neglect stress gradients (e.g., Xu et al., 2019; Yue et al., 2019). This contrasts with routine observations of stress gradients from industry data (Fig. 1A) and the fact that these gradients are considered in the well design of industrial operations (Lecampion et al., 2013; Mair et al., 2012). When this gradient is included in formulations, stress intensity varies around the fracture's tip-line (Fig. 2). Where K_c is exceeded, the upper tip-line advances. The contained fluid flows into this newly created fracture surface while the bottom edge of the fracture is pinched shut as the internal pressure drops. With a great enough volume this fluid movement maintains a critically stressed upper tip-line and the fracture reaches a state of 'self-sustaining propagation'. Fluid viscosity will cause some fluid to stay trapped in the tail trailing behind the fracture; if fluid viscosity is low enough, the contained fluid is virtually all transported. Provided the fracture's shape and volume are maintained, no additional forces, such as pressure from injection, are required to aid this state of propagation.

1.2 Analytical formulation

Secor and Pollard (1975) define in 2D the size and pressure inside a vertical fracture subject to $\Delta\gamma = (\rho_r - \rho_f)g$ such that at the upper tip $K_I^+ = K_c$ and at the lower tip $K_I^- = 0$. We derive an analytical expression for the fluid volume needed for a three-dimensional crack to propagate in a self-sustained manner.

K_I for a mode I penny-shaped fracture of radius c subject to a generic linear stress gradient can be expressed as the superposition of K_I for a penny-shaped fracture subject to a uniform pressure p_0:

$$K_I = \frac{2}{\pi} p_0 \sqrt{\pi c} \tag{1}$$

and that for a penny-shaped fracture subject to a linear pressure gradient $\Delta\gamma$ where pressure is equal to 0 at the fracture's midpoint (Tada et al., 2000, p. 355):

$$K_I^{\pm} = \pm \frac{4}{3\pi} \Delta\gamma c \sqrt{\pi c} \tag{2}$$

where the + refers to the propagating tip and the - to the basal tip. Requiring $K_I^- = 0$ results in $p_0 = 2\Delta\gamma c/3$ and thus:

$$p^{\pm} = \left(\frac{2}{3} \pm 1\right) \Delta\gamma c \tag{3}$$

Requiring $K_I^+ = K_c$ and rearranging for c yields:

$$c = \left(\frac{3\sqrt{\pi} K_c}{8\Delta\gamma}\right)^{2/3} \tag{4}$$

We note that the 2D plane strain critical length is $\approx 0.9c$. The volume of the crack can be calculated based on the equation for a crack pressurised by uniform pressure p_0, as the antisymmetric pressure contribution integrates to zero. Thus using (Tada et al., 2000):

$$V = \frac{8(1-\nu)}{3\mu} p_0 c^3 \tag{5}$$

results in:

$$V_c^{an} = \frac{(1-\nu)}{16\mu} \left(\frac{9\pi^4 K_c^8}{\cos(\theta)\Delta\gamma^5}\right)^{1/3} \tag{6}$$

This equation requires validation in order to evaluate the bias due to approximating the shape of the propagating crack as circular (Fig. 1D/E).

1.3 Numerical model

To simulate propagation, we use a 3D Boundary Element program where each element is a triangular dislocation with constant displacement (Fig. 2) (Nikkhoo & Walter, 2015). The program computes fracture opening and stress intensities, based on fracture shape, rock and fluid parameters and external stresses Davis et al. (2019). Our workflow during each iteration is as follows:

Figure 2. Numerical simulation of crack propagation (from left to right), looking at the fractures' face (left) and cross section (right). Grey points are edges that closed in the previous iteration.

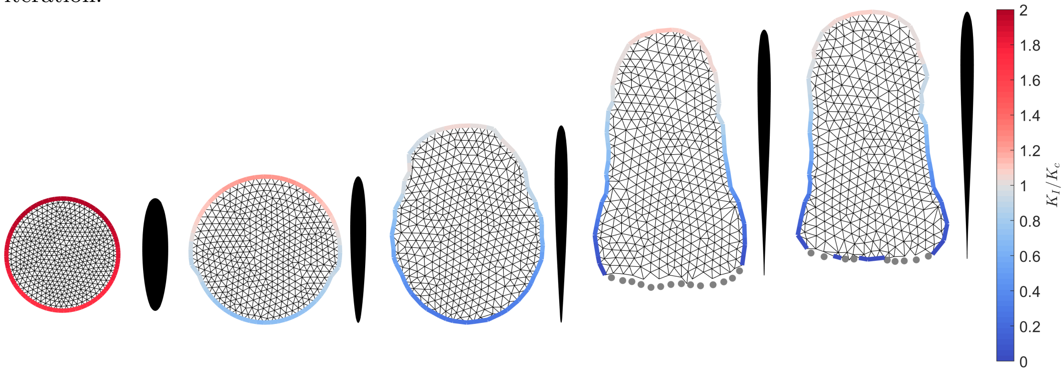

1. We invert for the uniform internal fluid pressure, p_0, necessary to open the crack to match the required volume against all external and internal tractions. Non-linear complementarity conditions are imposed such that the crack's faces cannot interpenetrate (Davis et al., 2019).
2. We calculate the crack opening and the stress intensity at the tipline using the method of Davis et al. (2019). In order to reduce artefacts, we smooth the stress intensity along the tip line by averaging the local K_I with its two neighbouring edges.
3. We calculate the advance or retreat of the tipline. At elements where K_I exceeds K_c, the tip-line will advance proportional to K_I/K_c. This approximation is akin to the "Paris fatigue law" (Lecampion et al., 2018). The maximum crack advance will occur at the triangle where K_I is maximum; this advance is set equal to the mesh's average triangle size. The triangular elements that close are removed. The simulation assumes the fluid is inviscid, and, as such, we cannot retrieve time-dependent propagation rates.
4. Once the fracture's edge has been updated, it is re-meshed and cleaned such that the triangles on the fractures tip-line are approximately equal size and isosceles (Da & Cohen-Steiner, 2019).

For a description of the numerical methods accuracy, see the appendix. We start the simulation with a vertical penny-shaped crack. We fix the number of elements, K_c, $\Delta\gamma$, μ, ν and the volume of fluid, V. We set the initial radius to $0.4c$, (Eq. 4). In our 350+ simulations we use variables spanning several orders of magnitude: G=190–5·10^{10}Pa, ν=0.25–0.49, $\Delta\gamma$=7.8·10^2–2.2·10^4Pa·m^{-1} and K_c=1-1·10^8Pa·m$^{0.5}$. We state the fracture has reached self-sustaining ascent when its upper tip has travelled $4c$ upwards.

For all simulations, independent of mesh sampling, we find that if $V = 0.7V_c^{an}$ the numerical code returns a trapped fracture and if $V = 0.8V_c^{an}$ the fracture always reaches self-sustaining propagation. Therefore, scaling Eq. 6 by 0.75 supplies the numerical estimate of V_c, independent of the scale we use:

$$V_c^{num} = 0.75\frac{(1-\nu)}{16\mu}\left(\frac{9\pi^4 K_c^8}{\cos(\theta)\Delta\gamma^5}\right)^{1/3} \tag{7}$$

For all cracks that reached self-sustaining propagation the horizontal and vertical lengths were greater than $\sim 0.6c$ and $\sim 1.14c$, respectively.

Figure 3. $V^*\mu$ vs K_c from Heimpel and Olson (1994). Eq. 7 predictions shown as black lines. The thickness of the grey filled patches represents the velocity of the crack as the volume increases, normalised by maximum observed velocity.

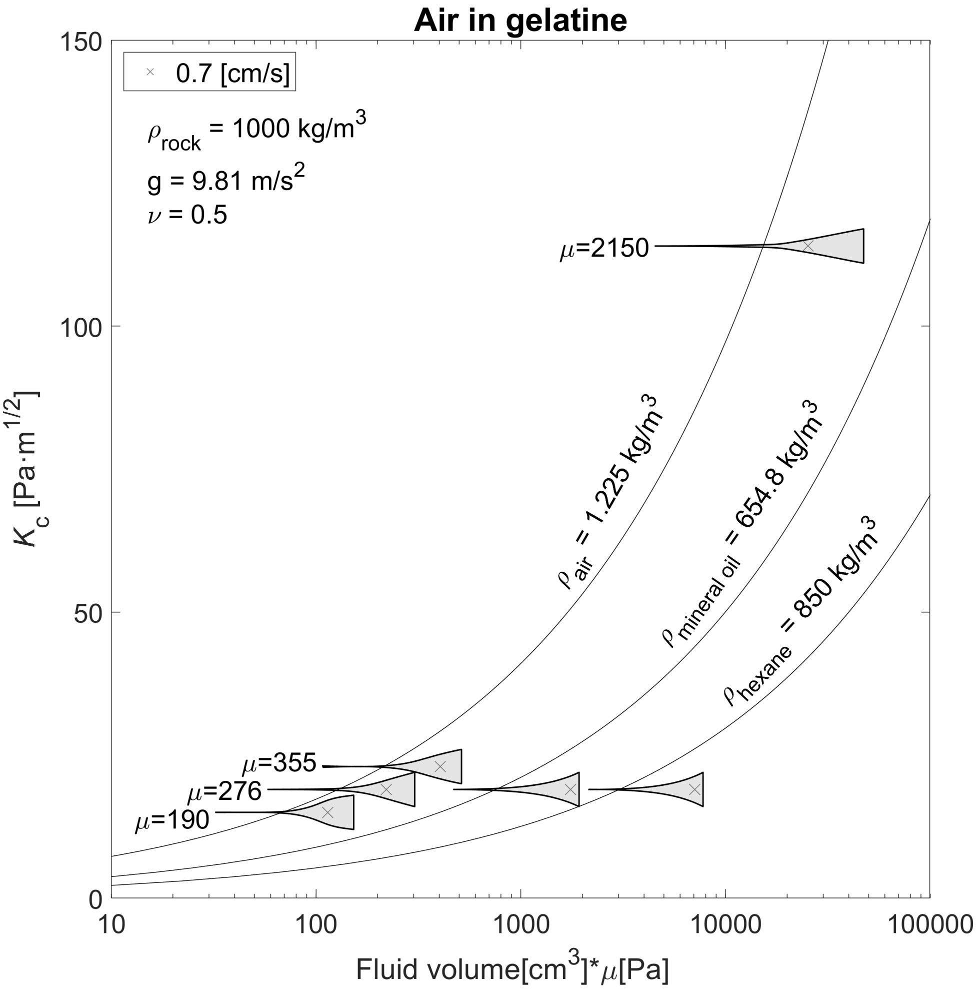

2 Applications

2.1 Analog gelatine experiments

The analog study of Heimpel and Olson (1994) inspects critical volumes of fluids ascending in gelatine blocks of different stiffness and fracture toughness (Fig. 3). The graph of volume vs speed from their experimental results shows a rapid increase in speed past a certain volume. The authors interpret that at velocities past $\sim 0.7\ cm/s$ (crosses in Fig. 3), the ascent transitions from a sub-critical propagation regime ($K_I < K_c$); where the fracture growth speed at the tip limits the velocity (Atkinson & Meredith, 1987), to a dynamic propagation regime. We test if our equation can predict volume of fluid that causes this transition in ascent speed. As Heimpel and Olson (1994) estimate K_c directly from this change in velocity, to verify that we can use this estimation, we calculate K_c differently; directly from the measured value of G. Strain energy release $\mathcal{G}$ increases with greater stiffness in gelatin solids: $\mathcal{G}$[N/m]$\approx 6.66{\cdot}10^{-4}G$[Pa] (Czerner et al., 2016). This second independent estimate of K_c lies within 5 Pa·m$^{1/2}$ of the original estimate. Using ρ_r=1000 kg·m^{-3}, ν=0.5 and setting μ, ρ_f and K_c to match the experiments of Heimpel and Olson (1994), we find that our value of V_c^{num} independently captures the point at which the velocity transitions, described above, supporting the previous interpretation that this describes the transition to dynamic fracture propagation.

2.2 Magmatic dykes

We consider magma propagation volumes at Piton de la Fournaise, La Réunion, to see how our equation matches observed dyke volumes. The volumes of the dyke intrusions observed between 1998-2016 range from 0.05-3.2·10^6·m^3 (Froger et al., 2004; Fukushima et al., 2005, 2010; Smittarello et al., 2019). Using $\rho_r - \rho_f$=100 kg·m^{-3}, μ=5 GPa, ν=0.25 and K_c ranging from 29 to 112 MPa·m$^{1/2}$ (Fukushima et al., 2010; Delaney & Pollard, 1981), we retrieve V_c^{num}=0.05·10^6 and 2·10^6·m^3, respectively. The critical volumes we estimate are consistent with the observed dyke sizes. As such our approximation predicts the correct scale in natural settings, provided K_c values estimated from field data are used, noting such field values appear to correct due to a number of additional processes that we have disregarded, instead of being representative of the rock strength at the scale of a laboratory sample.

2.3 Water injection into stiff rock

The UK government defines hydraulic fracturing as operations that use over 1,000 m^3 of fluid per frack stage. During a hydro-fracturing procedure, proppant is injected in the final phase to maintain an open fracture (e.g. spherical quartz grains). After the operation, not all injected fluid is recovered when the wellhead valve is opened: Vidic et al. (2013) report an average of only 10% fluid recovery in flowback waters, noting that this recovery volume decreases when shut-in times are longer. Using ρ_r=2700 kg·m^{-3}, ρ_f=1000 kg·m^{-3}, μ=8.9 GPa, ν=0.25 and K_c in the range 0.36–4.05 to 7–25 MPa·m$^{1/2}$, we obtain $V_c^{num} = 6{\cdot}10^{-2}$ and 500 m^3 respectively. These K_c values are for laboratory-sized shale samples from 100 to 1000 m confining pressure and effective K_c values estimated for veins in the field, respectively (Gehne et al., 2020; Olson, 2003). Current operations use volumes around double our highest predicted limit. Few observations attest to the fact that industrial operations can cause ascent of fluids in fractures. One such example, are the spectacular surface fissures created due to steam injection documented in Schultz (2016); additional examples can be found in Schultz et al. (2016). Geochemical data from aquifers above fracking operation sites has shown some evidence of the contamination of overlying units, which is attributed to poor well casing design, rather than fracture ascent (Vidic et al., 2013). Usually, microseismic monitoring of actual fracking operations show limited vertical extents of the fractures, however, these data are proprietary and methodological descriptions are scarce (Fisher & Warpinski, 2012). Experimental fracturing data is of little help as volumes injected are typically below or close to our volumetric limit, with injected volumes of 2 to 20 m^3 (Warpinski et al., 1982; Pandurangan et al., 2016).

Natural degassing, such as CO_2 in the Cheb basin, Czech Republic, has chemical signatures of fluids that have ascended over 20 km through the crust (Weinlich, 2014). Fracture driven ascent can explain this phenomena without the requirement of permanent highly conductive fluid pathways at great depths. Supercritical CO_2 at depth has a similar density to water, and as such may be a good natural analog for water filled fracture ascent. We saw that in analogue and magmatic examples Eq. 7 predicts the correct order of magnitude of critical volumes; at the same time, it appears that this equation is conservative for high volume water injection as fracture ascent in these settings has rarely been observed.

Figure 4. Processes that can hinder fracture ascent, K and V relate to effective K_c and V_c operating in Eq. 7

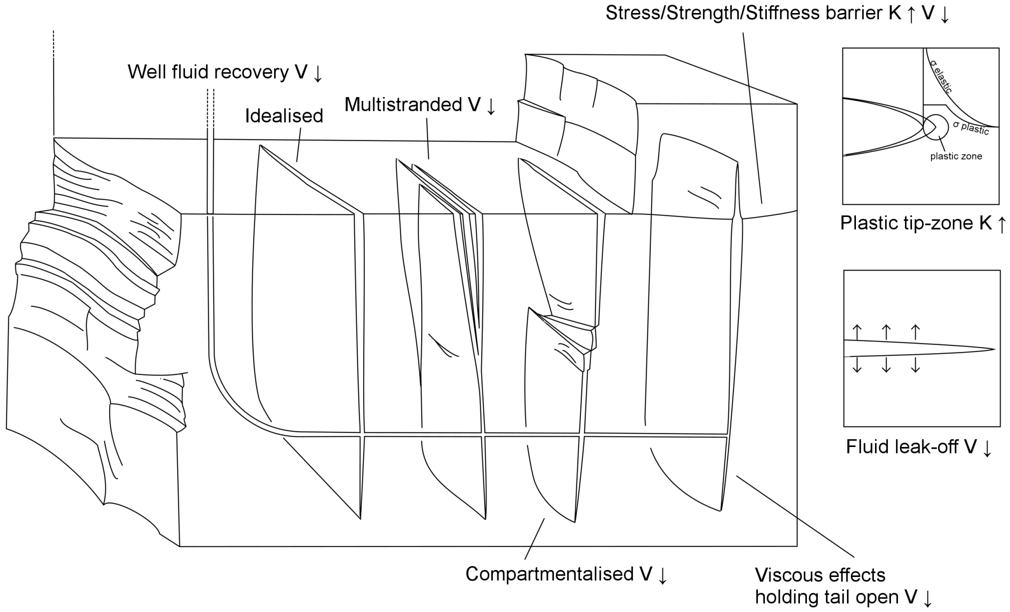

3 Discussion and conclusions

In summary, Eq. 7 provides an estimate of the minimum fluid volume for self-sustained propagation of fluid-filled fractures, ranging from cm to tens of km. V_c is dependent on $K_c^{8/3}$; since K_c is often poorly constrained V_c suffers from large uncertainties. Values of K_c obtained in laboratory experiments show a strong dependency on pressure and temperature. Field estimates of effective K_c from trapped fractures can be orders of magnitude larger. An effective way to estimate K_c in Eq. 7 incorporating all processes affecting the energy needed to extend the fracture at different scales would clearly be beneficial for any fracture mechanics based analysis of rock masses and the resultant interpretations.

In our derivation we have neglected the effects of viscosity. Whether these effects will dominate over toughness in determining fracture growth can be assessed by evaluating the time scale needed for the fluid pressure to equilibrate within the crack, as this will mean that viscous dissipation is low and crack growth will be toughness-dominated (Bunger & Detournay, 2007). The model of Bunger and Detournay (2007) assumes a constant injection rate with no stress gradients, we assume this still provides a rough estimate of the timescale until this transition. Typical industrial operations use fluid viscosity of 0.001-0.01 Pa·s, injection rates between 0.5-10 m^3/min and stiffness's of 10-40 GPa. Using low values of K_c from laboratory experiments in shale, 0.36 MPa·$m^{1/2}$, this transition time ranges between 1 minute to times exceeding the end of injection. Whereas, setting K_c higher, values for shale at depth, e.g. 4 MPa·$m^{1/2}$ this significantly reduces this range from milliseconds to a maximum of 5 hours. This suggests that, depending on K_c, Eq. 7 can be a relevant estimate of V_c^{num}, independent of viscous forces.

While theory and experiments support Eq. 7, this appears to be overly conservative in practice, as injections of quantities of fluid exceeding this do not result in significant ascent in most cases. In part, this discrepancy results from our simplification of the process, as mass conserving propagation in a homogeneous linear-elastic medium. Fig. 4 shows a schematic of processes not quantified in relation to critical fluid volumes which we review in detail below.

1. A series of mechanisms can reduce V during propagation and thus promote crack arrest. These include leak-off from the fractures faces, the fracture becoming multistranded/compartmentalised, fluid recovery (extraction), or fluid remaining in the tail of the fracture due to added proppant or viscous forces (Taisne & Tait, 2009).
2. Mechanisms that can lead to an effective increase of K_c, and thus also promote crack arrest, include plastic tip processes, the fracture entering in a zone of damage of the host rock (Sih et al., 1965; Kaya & Erdogan, 1980), or seismicity surrounding the fracture, causing reduction in the system's energy/blunting the fracture's tip (Rivalta et al., 2015).
3. Heterogeneous μ or K_c or stress barriers may also lead to arrest of fractures by deflection or promoting lateral growth (Maccaferri et al., 2011; Bunger & Lecampion, 2017; Warpinski et al., 1985),
4. Eq. 7 has a clear dependency on the fracture's dip. If the minimum compressive stress is vertical, this promotes flat lying fractures.

Quantification of processes acting to halt fracture ascent, especially in the context of the variables in our equation, are critical to understand which volumetric limits can be deemed safe. In particular, the gradient in stress with depth must be included to assess this process. Without such quantification, regulation of this industrial process will continue to rely on empirical evidence for safe rates, volumes and depths from select operations that may not be representative.

Appendix A Numerical

A1 Numerical accuracy

We verify that our method to compute K_I is independent of crack shape and boundary condition. Previously this was only compared to solutions for a circular crack subject to uniform stresses (Davis et al., 2019). We compare this to the analytical solution for the stress intensity around an elliptical crack, subject to a superposition of uniform pressure and a linear gradient of stress, such that, at the basal tip, $K_I = 0$ (Fig. 1) (Atroshchenko et al., 2009). We note that under a stress gradient, K_I for vertically aligned elliptical cracks is not maximal at its upper tip, due to the reduction in crack surface area proximal to this edge.

For a mesh with 650 triangles (Fig. A1A/B), the greatest vertical separation between the numerical points and the analytical line is 0.09. For this test we required the edge points of the mesh's triangles, not the midpoints of the triangles edge where K_I is calculated, to lie on the tip-line defined by the analytical solution. For a mesh with 1500 triangles (Fig. A1C/D), the maximum vertical distance from the analytical solution of is 0.06, noting that greater sampling does not necessarily converge to a improved accuracy, see appendix of Davis et al. (2019).

As a further test of numerical accuracy, we compare how well the numerical method approximates the opening volume of a penny shaped crack subject to tension (Tada et al., 2000). We find a sampling of 650 triangles overestimates the volume by 5.2%, by increasing the triangle count to 1500 this drops to 3.5%.

Acknowledgments

The authors would like to thank the reviewers Meredith Townsend and Dmitry Garagash for their insightful and constructive reviews of the manuscript. T Davis is funded by the DFG-ICDP grant N. RI 2782/3-1. The code used for the numerical analysis of this study was the open source code `https://doi.org/10.5281/zenodo.3694163` with an interface with the Computational Geometry Algorithms Library software (C++) for meshing.

References

Atkinson, B. K., & Meredith, P. G. (1987). The theory of subcritical crack growth with applications to minerals and rocks. *Fracture mechanics of rock*, *2*, 111–166.

Atroshchenko, E., Potapenko, S., & Glinka, G. (2009). Stress intensity factor for an embedded elliptical crack under arbitrary normal loading. *International Journal of Fatigue*, *31*(11-12), 1907–1910.

Bell, J., Price, P., & McLellan, P. (1990). In-situ stress in the western canada sedimentary basin. *Bulletin of Canadian Petroleum Geology*, *38*(1), 157–157.

Bunger, A., & Detournay, E. (2007). Early-time solution for a radial hydraulic fracture. *Journal of engineering mechanics*, *133*(5), 534–540. doi: 10.1061/(ASCE)0733-9399(2007)133:5(534)

Bunger, A., & Lecampion, B. (2017). *Four critical issues for successful hydraulic fracturing applications* (Tech. Rep.). CRC Press.

Czerner, M., Fasce, L. A., Martucci, J. F., Ruseckaite, R., & Frontini, P. M. (2016). Deformation and fracture behavior of physical gelatin gel systems. *Food Hydrocolloids*, *60*, 299–307.

Da, T. K. F., & Cohen-Steiner, D. (2019). Advancing front surface reconstruction. In *CGAL user and reference manual* (4.14.1 ed.). CGAL Editorial Board. Retrieved from `https://doc.cgal.org/4.14.1/Manual/packages.html#PkgAdvancingFrontSurfaceReconstruction`

Dahm, T. (2000). On the shape and velocity of fluid-filled fractures in the earth. *Geophysical Journal International*, *142*(1), 181–192. doi: 10.1046/j.1365-246x.2000.00148.x

Das, S. B., Joughin, I., Behn, M. D., Howat, I. M., King, M. A., Lizarralde, D., & Bhatia, M. (2008). Fracture propagation to the base of the greenland ice sheet during supraglacial lake drainage. *Science*, *320*(5877), 778–781. doi: 10.1126/science.1153360

Davis, T., Healy, D., & Rivalta, E. (2019). Slip on wavy frictional faults: Is the 3rd dimension a sticking point? *Journal of Structural Geology*, *119*, 33–49. doi: 10.1016/j.jsg.2018.11.009

Delaney, P. T., & Pollard, D. D. (1981). *Deformation of host rocks and flow of magma during growth of minette dikes and breccia-bearing intrusions near ship rock, new mexico* (Tech. Rep.). USGPO. doi: 10.3133/pp1202

EPA, U. (2016). Hydraulic fracturing for oil and gas: Impacts from the hydraulic fracturing water cycle on drinking water resources in the united states. *Washington, DC: US Environmental Protection Agency, EPA/600/R-16/236F*.

Fisher, M. K., & Warpinski, N. R. (2012). Hydraulic-fracture-height growth: Real data. *SPE Production & Operations*, *27*(01), 8–19. doi: 10.2118/145949-PA

Froger, J.-L., Fukushima, Y., Briole, P., Staudacher, T., Souriot, T., & Villeneuve, N. (2004). The deformation field of the august 2003 eruption at piton de la fournaise, reunion island, mapped by asar interferometry. *Geophysical research letters*, *31*(14). doi: 10.1029/2004GL020479

Fukushima, Y., Cayol, V., & Durand, P. (2005). Finding realistic dike models from interferometric synthetic aperture radar data: The february 2000 eruption at piton de la fournaise. *Journal of Geophysical Research: Solid Earth*, *110*(B3). doi: 10.1029/2004JB003268

Fukushima, Y., Cayol, V., Durand, P., & Massonnet, D. (2010). Evolution of magma conduits during the 1998–2000 eruptions of piton de la fournaise volcano, réunion island. *Journal of Geophysical Research: Solid Earth*, *115*(B10). doi: 10.1029/2009JB007023

Gehne, S., Forbes Inskip, N., Benson, P., Meredith, P., & Koor, N. (2020). Fluid-driven tensile fracture and fracture toughness in nash point shale at elevated pressure. *Journal of Geophysical Research: Solid Earth*, e2019JB018971.

Heimpel, M., & Olson, P. (1994). Buoyancy-driven fracture and magma transport through the lithosphere: models and experiments. In *International geophysics* (Vol. 57, pp. 223–240). Elsevier.

Kaya, A., & Erdogan, F. (1980). Stress intensity factors and cod in an orthotropic strip. *International Journal of Fracture*, *16*(2), 171–190. doi: 10.1007/BF00012620

Lecampion, B., Bunger, A., Kear, J., & Quesada, D. (2013). Interface debonding driven by fluid injection in a cased and cemented wellbore: Modeling and experiments. *International Journal of Greenhouse Gas Control*, *18*, 208–223. doi: 10.1016/j.ijggc.2013.07.012

Lecampion, B., Bunger, A., & Zhang, X. (2018). Numerical methods for hydraulic fracture propagation: a review of recent trends. *Journal of natural gas science and engineering*, *49*, 66–83. doi: 10.1016/j.jngse.2017.10.012

Maccaferri, F., Bonafede, M., & Rivalta, E. (2011). A quantitative study of the mechanisms governing dike propagation, dike arrest and sill formation. *Journal of Volcanology and Geothermal Research*, *208*(1-2), 39–50. doi: 10.1016/j.jvolgeores.2011.09.001

Mair, R., Bickle, M., Goodman, D., Koppelman, B., Roberts, J., Selley, R., … Younger, P. (2012). Shale gas extraction in the uk: a review of hydraulic fracturing.

Nikkhoo, M., & Walter, T. R. (2015). Triangular dislocation: an analytical, artefact-free solution. *Geophysical Journal International*, *201*(2), 1119–1141.

Okamoto, A., & Tsuchiya, N. (2009). Velocity of vertical fluid ascent within vein-forming fractures. *Geology*, *37*(6), 563–566. doi: 10.1130/G25680A.1

Olson, J. E. (2003). Sublinear scaling of fracture aperture versus length: an exception or the rule? *Journal of Geophysical Research: Solid Earth*, *108*(B9). doi: 10.1029/2001JB000419

Pandurangan, V., Chen, Z., & Jeffrey, R. G. (2016). Mapping hydraulic fractures from tiltmeter data using the ensemble kalman filter. *International Journal for Numerical and Analytical Methods in Geomechanics*, *40*(4), 546–567. doi: 10.1002/nag.2415

Rivalta, E., & Dahm, T. (2006). Acceleration of buoyancy-driven fractures and magmatic dikes beneath the free surface. *Geophysical Journal International*, *166*(3), 1424–1439. doi: 10.1111/j.1365-246X.2006.02962.x

Rivalta, E., Taisne, B., Bunger, A., & Katz, R. (2015). A review of mechanical models of dike propagation: Schools of thought, results and future directions. *Tectonophysics*, *638*, 1–42. doi: 10.1016/j.tecto.2014.10.003

Schultz, R. A. (2016). Causes and mitigation strategies of surface hydrocarbon leaks at heavy-oil fields: examples from alberta and california. *Petroleum Geoscience*, *23*(2), 231–237. doi: 10.1144/petgeo2016-070

Schultz, R. A., Mutlu, U., & Bere, A. (2016). Critical issues in subsurface integrity. In *50th us rock mechanics/geomechanics symposium.*

Secor, D. T., & Pollard, D. D. (1975). On the stability of open hydraulic fractures in the earth's crust. *Geophysical Research Letters*, *2*(11), 510–513. doi: 10.1029/GL002i011p00510

Sih, G. C., Paris, P., & Irwin, G. R. (1965). On cracks in rectilinearly anisotropic bodies. *International Journal of Fracture Mechanics*, *1*(3), 189–203. doi: 10.1007/BF00186854

Smittarello, D., Cayol, V., Pinel, V., Peltier, A., Froger, J.-L., & Ferrazzini, V. (2019). Magma propagation at piton de la fournaise from joint inversion of insar and gnss. *Journal of Geophysical Research: Solid Earth*, *124*(2), 1361–1387. doi: 10.1029/2018JB016856

Tada, H., Paris, P., & Irwin, G. (2000). *The stress analysis of cracks handbook; third edition.* New York: ASME Press.

Taisne, B., & Tait, S. (2009). Eruption versus intrusion? arrest of propagation of constant volume, buoyant, liquid-filled cracks in an elastic, brittle host. *Journal of Geophysical Research: Solid Earth*, *114*(B6). doi: 10.1029/2009JB006297

Taisne, B., Tait, S., & Jaupart, C. (2011). Conditions for the arrest of a vertical propagating dyke. *Bulletin of Volcanology*, *73*(2), 191–204. doi: https://doi.org/10.1007/s00445-010-0440-1

Tolstoy, M., Cowen, J., Baker, E., Fornari, D., Rubin, K., Shank, T., ... Love, B. (2006). A sea-floor spreading event captured by seismometers. *Science*, *314*(5807), 1920–1922. doi: 10.1126/science.1133950

Vidic, R. D., Brantley, S. L., Vandenbossche, J. M., Yoxtheimer, D., & Abad, J. D. (2013). Impact of shale gas development on regional water quality. *Science*, *340*(6134), 1235009. doi: 10.1126/science.1235009

Warpinski, N. R., Branagan, P., & Wilmer, R. (1985). In-situ stress measurements at us doe's multiwell experiment site, mesaverde group, rifle, colorado. *Journal of petroleum technology*, *37*(03), 527–536. doi: 10.2118/12142-PA

Warpinski, N. R., Schmidt, R. A., & Northrop, D. A. (1982). In-situ stresses: the predominant influence on hydraulic fracture containment. *Journal of Petroleum Technology*, *34*(03), 653–664. doi: 10.2118/8932-PA

Weinlich, F. (2014). Carbon dioxide controlled earthquake distribution pattern in the nw bohemian swarm earthquake region, western eger rift, czech republic–gas migration in the crystalline basement. *Geofluids*, *14*(2), 143–159. doi: 10.1111/gfl.12058

Xu, W., Prioul, R., Berard, T., Weng, X., & Kresse, O. (2019). Barriers to hydraulic fracture height growth: A new model for sliding interfaces. In *Spe hydraulic fracturing technology conference and exhibition.* doi: 10.2118/194327-MS

Yue, K., Olson, J. E., & Schultz, R. A. (2019). The effect of layered modulus on hydraulic-fracture modeling and fracture-height containment. *SPE Drilling & Completion*. doi: 10.2118/195683-PA

Figure A1. Stress intensity factor approximation using the 3D displacement discontinuity method. A/C) Elliptical crack meshed with 650/1500 triangles respectively, B/D) Numerical (dots) and analytical (solid line) results. Results are normalised relative to the maximum analytical value of K_I.